Available online at www.sciencedirect.com
SCIENCE DIRECT®
Applied Energy 83 (2006) 989–1003
APPLIED ENERGY
www.elsevier.com/locate/apenergy

Influence of a building's integrated-photovoltaics on heating and cooling loads

Yiping Wang *, Wei Tian, Jianbo Ren, Li Zhu, Qingzhao Wang

School of Chemical Engineering and Technology, Tianjin University, Tianjin 300072, China

Received 7 July 2005; received in revised form 12 September 2005; accepted 2 October 2005
Available online 2 December 2005

Abstract

Building integrated photovoltaics (BIPV) has the potential to become a major source of renewable energy in the urban environment. BIPV has significant influence on the heat transfer through the building envelope because of the change of the thermal resistance by adding or replacing the building elements. Four different roofs are used to assess the impacts of BIPV on the building's heating-and-cooling loads; namely ventilated air-gap BIPV, non-ventilated (closed) air-gap BIPV, closeroof mounted BIPV, and the conventional roof with no PV and no air gap. One-dimensional transient models of four cases are derived to evaluate the PV performances and building cooling-and-heating loads across the different roofs in order to select the appropriate PV building integration method in Tianjin, China. The simulation results show that the PV roof with ventilated air-gap is suitable for the application in summer because this integration leads to the low cooling load and high PV conversion efficiency. The PV roof with ventilation air-gap has a high time lag and small decrement factor in comparison with other three roofs and has the same heat gain as the cool roof of absorptance 0.4. In winter, BIPV of non-ventilated air gap is more appropriate due to the combination of the low heating-load through the PV roof and high PV electrical output.

Keywords: BIPV; Cooling load; Heating load; Heat transfer

* Corresponding author. Tel./fax: +86 2227404771.
E-mail address: tjtianjin@yahoo.com.cn (Y. Wang).

0306-2619/$ - see front matter © 2005 Elsevier Ltd. All rights reserved.
doi:10.1016/j.apenergy.2005.10.002

Nomenclature

A	PV area (m^2)
A_c	cross-section area of the duct (m^2)
C	specific heat (J/kg K)
C_p	wind-pressure coefficients
d	width (m)
D	gap of the duct (m)
D_h	hydraulic diameter of the duct (m)
f	friction factor
F	view factor
g	acceleration due to gravity (m/s^2)
G	solar radiation (W/m^2)
h	heat-transfer coefficient (W/m^2 K)
h_n	natural convection heat-transfer coefficient (W/m^2 K)
I_{mp}	PV current at maximum power point (A)
k	thermal conductivity (W/m K)
K_f	pressure-loss coefficient
L	duct length (m)
m	mass flow-rate (kg/s)
M	mass (kg)
Nu	Nusselt number
P_{mp}	PV power at maximum power (W)
q	rate of heat exchange (W)
R	thermal resistance
Ra	Rayleigh number
Re	Reynolds number
T	temperature (°C)
U_{mp}	PV voltage at maximum power (V)
V	wind speed (m/s)

Greeks

α	solar absorptance
α_d	thermal diffusivity of roof (m^2/s)
β	coefficient of thermal expansion of air (1/K)
δ	Stefan–Boltzmann constant
ε	surface emissivity
θ	PV tilt angle
ρ	reflectance or density (kg/m^3)

Subscripts

a	ambient
c	convection heat-transfer
d	roof or conduction heat-transfer
e	roof's exterior surface
f	air in the gap

g	glass cover of PV
gr	ground
h	room
i	roof interior surface
r	radiation heat-transfer
s	PV cell
t	back sheet of PV
w	wind

1. Introduction

In China, building energy consumption accounts for approximately 27.6% of the total energy use and is increasing [1]. Solar energy systems play an important role in reducing building energy consumption [2]. Building integrated photovoltaics (BIPV) replaces conventional building elements such as roof tiles, asphalt shingles, facade elements, and shading devices with photovoltaic modules that perform the same function but also provides electrical power.

It is evident that BIPV has significant influence on the heat transfer through the building envelope and its consequent effect on the building's cooling and heating loads. Relative little research has been published on the impact of BIPV on the building's heating-and-cooling loads. Ventilated walls, facades and roofs, if well designed, can help reduce considerably the summer thermal-loads due to direct solar radiation [3]. The combination of PV and ventilated roofs not only improves the PV conversion efficiency, but also decreases the cooling load through the roofs. Brinkworth et al. [4] found that the reduction of PV temperature up to 20 K can be obtained by heat transfer to an air flow induced by buoyancy in a duct behind the PV component, with a significant increase in the electrical output and reduction of heat gain into the building. Yang et al. [5] revealed that the cooling-load component through a PV roof with the ventilation gap is about 35% compared with the load of a conventional roof. But Mei et al. [6] reported different results that the cooling loads are marginally higher with the PV facade with the ventilation gap for all locations considered, whereas the impact of the facade on the heating load depends critically on location.

Different types of BIPV have various influences on the building cooling-and-heating loads. This paper developed a one-dimensional transient heat-transfer model for integrating PV systems into buildings. Then comparisons of PV performance and building cooling and heating loads are made according to the simulation results. The comparisons of heat gain through PV roof with ventilated air-gap and cool roof (high-reflective roof) are also described.

2. BIPV model

In this section, four models for different roofs are described to evaluate the PV performance and building cooling and heating loads across them. The four various roofs are

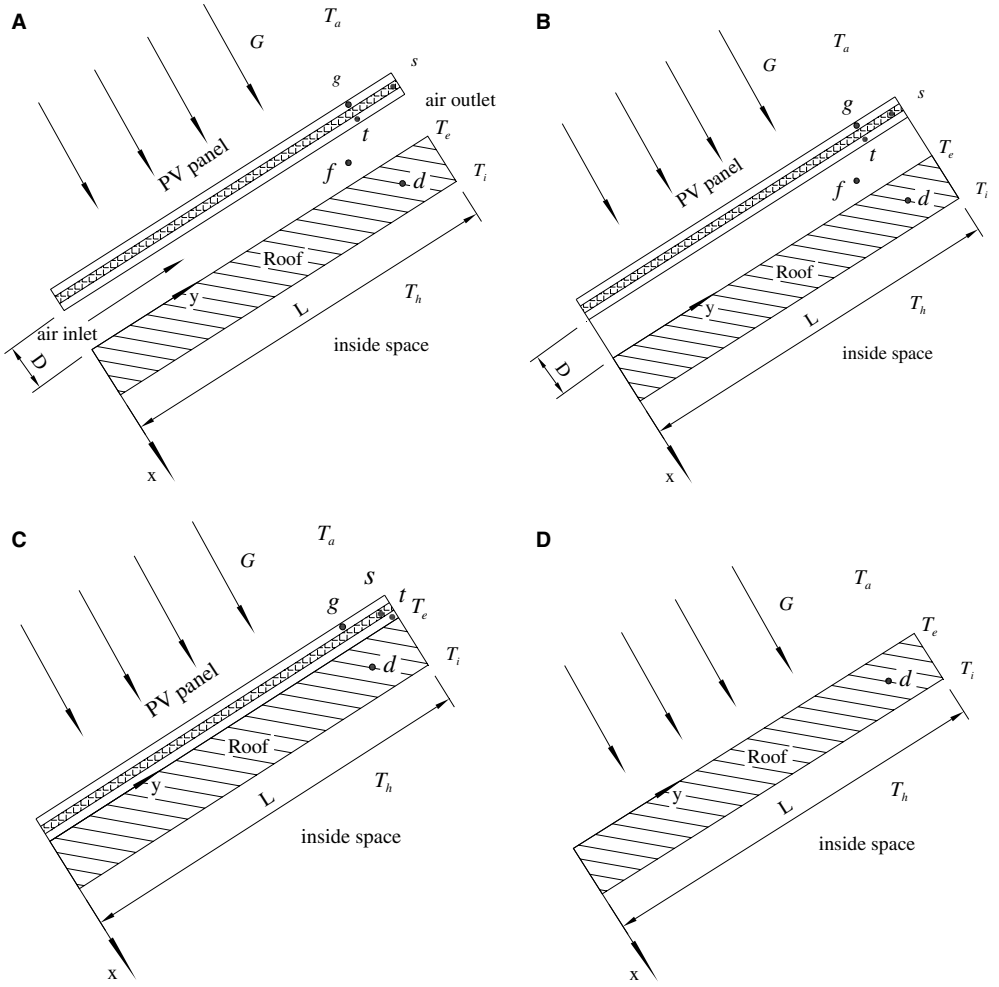

Fig. 1. Cross-section of different roofs (A – ventilated air gap BIPV, B – non-ventilated air gap BIPV, C – close mounted BIPV, D – conventional roof).

ventilated air-gap (A), non-ventilated (closed) air-gap (B), closeroof mounted (C), and the normal roof (D) that has no PV and no ventilation gap, as shown in Fig. 1.

2.1. Model of PV roof with ventilated air-gap (A)

2.1.1. Thermal model of BIPV

2.1.1.1. Energy balance of PV module. As denoted in Fig. 1A, the nodes g, s, and t, respectively, represent the glass cover of the PV module, the PV cell, and the PV back sheet. The node f is for the air in the gap and the node d is for the roof: T_e and T_i are the exterior and interior surface temperatures of the roof. Fig. 2 illustrates the energy flow through the PV roof system with a ventilation gap based on the R-C circuit representation.

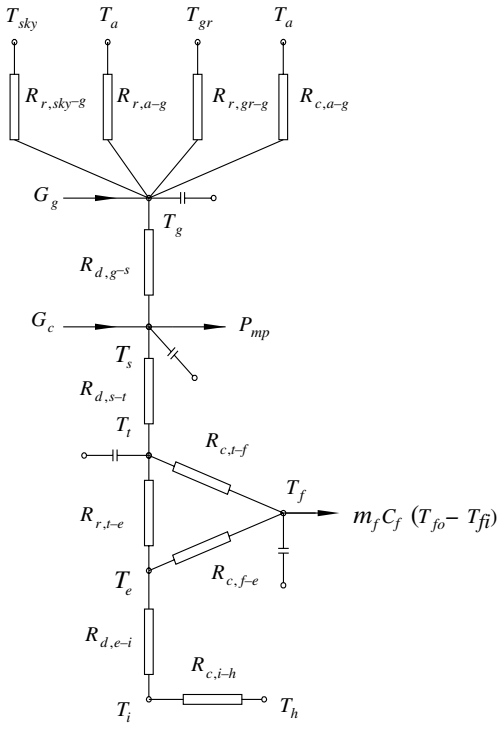

Fig. 2. Energy flow of BIPV with ventilated air-gap.

For the transparent cover,

$$M_g C_g \frac{dT_g}{dt} = G\alpha_g A(1-\rho_{o,g}) + h_w A(T_a - T_g) + h_{gs} A(T_s - T_g) + q_{r,ga}, \tag{1}$$

where the heat-transfer coefficient between the glass cover and the solar cells is

$$h_{gs} = 1 \Big/ \left(\frac{d_g/2}{k_g} + \frac{d_s/2}{k_s}\right). \tag{2}$$

The convection coefficient due to wind is given by [8]

$$h_w = \sqrt{h_n^2 + (2.38V^{0.89})^2}. \tag{3}$$

The natural-convection component is

$$h_n = 9.482 \frac{\sqrt[3]{|T_g - T_a|}}{7.328 - |\cos\theta|} \tag{4}$$

when the heat flow is upwards and

$$h_n = 1.810 \frac{\sqrt[3]{|T_g - T_a|}}{1.382 + |\cos\theta|} \tag{5}$$

when the heat flow is downwards.

The longwave radiation portion $q_{r,ga}$ of the heat balance is split into the three parts: exchange to air, exchange to sky, and exchange to ground

$$q_{r,ga} = A\varepsilon_g\delta\left[F_a\left(T_a^4 - T_g^4\right) + F_{sky}\left(T_{sky}^4 - T_g^4\right) + F_{gr}\left(T_{gr}^4 - T_g^4\right)\right]. \tag{6}$$

It is assumed that the surface ground temperature T_{gr} equals the air temperature T_a.

The sky temperature is calculated as a function of outdoor air temperature [8]

$$T_{sky} = 0.0552(T_a + 273.15)^{1.5}. \tag{7}$$

The calculation of three view factors is based on the PV tilt [7]

$$F_{sky} = \frac{1+\cos\theta}{2}\cos(\theta/2), \quad F_{gr} = (1-\cos\theta)/2, \quad F_a = 1 - F_{sky} - F_{gr}. \tag{8}$$

For the solar cells,

$$M_sC_s\frac{dT_s}{dt} = G(1-\rho_{o,g})(1-\alpha_g)\alpha_s + h_{st}A(T_t - T_s) + h_{gs}A(T_g - T_s) - P_{mp}. \tag{9}$$

The heat-transfer coefficient between the solar cells and the back sheet of PV is given by

$$h_{st} = 1\Big/\left(\frac{d_t/2}{k_t} + \frac{d_s/2}{k_s}\right). \tag{10}$$

For the back sheet of PV,

$$M_tC_t\frac{dT_t}{dt} = h_{st}A(T_s - T_t) + h_{tf}A(T_f - T_t) + A\delta\left(T_e^4 - T_t^4\right)/(1/\varepsilon_t + 1/\varepsilon_e - 1). \tag{11}$$

The convective heat-transfer coefficient between the PV rear-plate and the air in the gap can be obtained from [9]

$$h_{tf} = Nuk_f/D_h = (5.801 + 0.086\,ReD_h/L)k_f/D_h. \tag{12}$$

2.1.1.2. Heat transfer and flow of air in the gap.

For the air in the gap

$$M_fC_f\frac{dT_f}{dt} = h_{fe}A(T_e - T_f) + h_{tf}A(T_t - T_f) - m_fC_f(T_{fo} - T_{fi}). \tag{13}$$

It is assumed that convective heat-transfer coefficient h_{tf} on the rear plate of the PV is equal to h_{fe} on the roof's exterior surface. Assuming a linear heat rise in the air gap

$$T_f = (T_{fo} + T_{fi})/2. \tag{14}$$

The air flow rate in the gap caused by buoyancy and wind pressure is given by [10],

$$m_f = \rho_fA_c\sqrt{\frac{2\beta(T_{fo} - T_{fi})Lg\sin\theta + C_pV}{K_{f1} + K_{f2} + fL/D_h}}(T_{fo} + T_{fi})/2, \tag{15}$$

where V is the wind speed, K_{f1} and K_{f2} are the inlet and outlet pressure-loss coefficient and C_p is the wind-pressure coefficient. An average value of 0.25 is used from the literature [10]. The air has a mass flow rate m_f, enters the air duct at temperature T_{fi} which is approximately equal to the ambient air temperature and leaves with a higher temperature T_{fo}.

2.1.1.3. Heat transfer of roof. It is assumed that the heat transfer through the roof is one-dimensional unsteady heat-conduction

$$\frac{\partial T}{\partial t} = \alpha_d \frac{\partial^2 T}{\partial x^2}. \tag{16}$$

The boundary conditions in Eq. (16) are resulted from the following expression:

$$-k_d \left.\frac{\partial T}{\partial x}\right|_{x=0} = h_{fe}(T_e - T_f) + \delta\left(T_e^4 - T_t^4\right)/(1/\varepsilon_t + 1/\varepsilon_e - 1), \tag{17}$$

$$-k_d \left.\frac{\partial T}{\partial x}\right|_{x=d_d} = h_{ih}(T_i - T_h). \tag{18}$$

The indoor space is characterized by a specified internal temperature T_h, 24 °C, coupled to the interior surface by a heat-transfer coefficient [11].

2.1.2. PV electrical-performance model

The Sandia electrical performance model, described by King et al. [12], has evolved over many years at Sandia National Laboratories (SNL), and it has been extensively applied and validated for virtually all photovoltaic technologies now commercially available. The Sandia model consists of a series of empirical relationships with coefficients that are derived from actual testing. There are several climate and solar orientation inputs to the model that include incident beam-solar, incident diffuse-solar, solar angle of incidence, air mass, and elevation. The maximum power output from the PV module can be obtained from

$$P_{mp} = I_{mp} \cdot V_{mp}. \tag{19}$$

The calculation methods of I_{mp} and V_{mp} are described in detail in [12]. Both the electrical current generated by a module and its voltage are independently influenced by the operating temperature. Then it is important to predict accurately the PV module temperature. In the SNL thermal model, four different mounting configurations of BIPV are open rack, close roof mount, insulated back, and tracker. In the case of the air flow in the gap, these parameters are not available. The thermal model of the last section is used to calculate the PV module temperature.

2.1.3. Radiant time series (RTS) load-model

The radiant time series method is a new method for performing design cooling load calculation, derived from the heat-balance method [13]. The RTS method is well suited for use in a spreadsheet. The conduction transfer function is replaced with periodic response factors to calculate the hourly convective heat-gain in a wall or roof. The heat gain through the roof can also be determined by Eq. (18). According to the radiant time series, heat gain is split into radiative and convective portions. The radiant time factors are used to convert the radiant portion of hourly heat-gains to hourly cooling-loads based on the current and past values of radiative heat-gains:

$$Q_\theta = r_0 q_\theta + r_1 q_{\theta-\delta} + r_2 q_{\theta-2\delta} + \cdots + r_{23} q_{\theta-23\delta}, \tag{20}$$

where Q_q is the cooling load (Q) for the current hour (q), q_q is heat gain for the current hour, q_{q-nd} is heat gain n hours ago, and r_0, r_1, etc. are radiant time-factors. Radiant

time-factors can be achieved from the PRF-RTF Generator [14]. The latter calculates the periodic response factor (PRF) and radiant time factor (RTF) required by ASHRAE radiant time series load calculation method.

In order to evaluate the influence of BIPV on the building's cooling and heating loads, the total model consist of the BIPV thermal model, PV electrical performance model, and RTS cooling-load model.

2.2. Model of the PV roof with non-ventilated (closed) air-gap (B)

The equations for the case of the PV roof with closed air-gap are largely the same as the model for the PV roof with ventilated air-gap. The differences between them are the absence of the third term in Eq. (13) and the convective heat-transfer coefficient on the PV back sheet and the exterior surface of the roof is determined by [15]

$$Nu = 1 + 1.44\left[1 - \frac{1708}{Ra\cos\theta}\right]\left\{1 - \frac{1708(\sin 1.8\theta)^{1.6}}{Ra\cos\theta}\right\} + \left[\left(\frac{Ra\cos\theta}{5830}\right)^{1/3} - 1\right], \quad (21)$$

where the term in the square brackets is set equal to zero if the quantity within these brackets is negative.

2.3. Model of PV with closeroof mount (C)

In contrast to the PV roof with a ventilated or non-ventilated air gap, the model of a PV close roof mounted is relatively simple. For the energy-balance equation (11) of the rear plate of the PV, the convective and radiative heat-transfers are replaced with the conduction heat-transfer between the rear plate of the PV and the exterior surface of the roof, which leads to the disappearance of Eqs. (12) → (15).

2.4. Model of the roof with no ventilation and no PV (D)

The boundary condition of the roof becomes

$$-k_d \left.\frac{\partial T}{\partial x}\right|_{x=0} = G\alpha_e + h_w(T_e - T_a) + q_{r,ea}/A. \quad (22)$$

Eqs. (3)–(8) are still retained except for using T_e instead of T_g.

3. Solution procedures

For complex boundary-conditions and arbitrary initial temperature-distributions, the analytical solution became very involved and numerical methods are much more convenient. Computation for a given period begins with assumed initial conditions at midnight that all temperatures are equal to ambient temperature. To obtain the periodic steady-state solution, the calculation in all cases continues for 10 days, eliminating any error associated with initial transients. Three point central-difference [16] in space is employed when solving Eq. (16). The time discretization is calculated by the function ode15s in Matlab that is a variable-order solver based on the numerical differentiation

formulae, which are related to, but are more efficient than, the backward differentiation formulae [17].

Suppose that the roof structure is the same as the No. 13 roof given in ASHRAE [11]. The roof structure consists of a 12 mm slag or stone, 10 mm felt and membrane, 50 mm insulation and 150 mm concrete from outside to inside. The PV module is a Photowatt PW1000 consisting of a low-iron tempered glass sheet on front and a Tedlar back sheet. The thermal properties for the PV module [18] and roof [11] are listed in Table 1. The other parameters [19] used in the simulation are listed in Table 2. The building is located in Tianjin, China and the design conditions [20,21] are as follows:

Latitude: 39.13°N	Longitude: 117.2°E
Altitude: 3.3 m	Daily range: 8.1 °C
Ground reflectivity: 0.2	Zone air-temperature: 24 °C
Winter wind-speed: 3.1 m/s	Summer wind-speed: 2.6 m/s
Winter outdoor design-temperature: −11 °C	
Summer outdoor design-temperature: 33.4 °C	

The ambient conditions during the day were presented in Fig. 3.

Table 1
The thermal properties used in simulations

Material	Conductivity (W/(m K))	Density (kg/m^3)	Specific heat (J/(kg K))	Width (mm)
PV module				
Glass cover	1.04	2500	835	4
PV cell	150	1650	700	0.3
Back sheet	0.14	1475	1130	5
Roof structure				
Slag or stone	1.436	881	1670	11.989
Felt and membrane	0.19	1121	1670	10.008
Insulation	0.043	91	841	51.003
Concrete	1.731	2243	841	150.013

Table 2
Values of parameters used in simulations

Parameters	Value
α_g	0.06
ε_g	0.9
ε_c	0.9
$\rho_{o,g}$	0.04
A	4 m^2
α_c	0.9
ε_t	0.893
θ	40°
L	2.5 m
D	200 mm

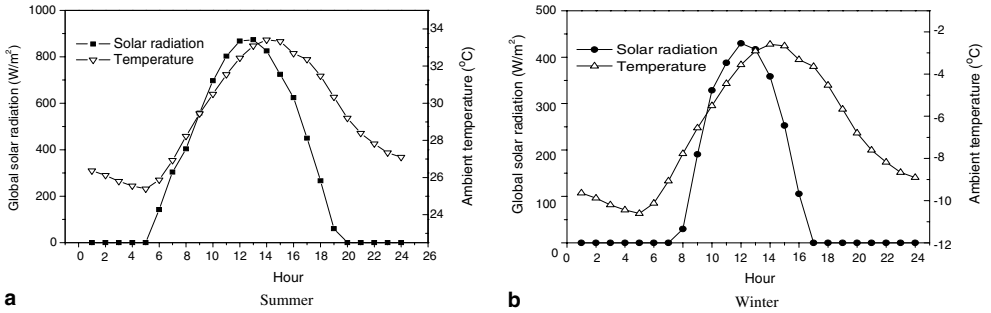

Fig. 3. Ambient conditions as a function of time.

4. Results and discussion

The results of simulations are summarized in Table 3.

4.1. The effect of the different roofs on the cooling load

4.1.1. The effects of the different roofs on the time lag and decrement factor

The time it takes for a heat wave to propagate from the outer surface to the inner surface, i.e. the 'time lag' and the decreasing ratio of its amplitude during this process is the 'decrement factor' [22]. The time lag and decrement factor are very important characteristics to determine the heat-storage capabilities of any material and strongly affect the indoor climate. Envelopes with high time-lags and small decrement-factors give comfortable inside temperatures even if the outside is very hot [23]. Simulation values of time lags of roofs A, B, C, and D are 7, 7, 5, and 6 h, respectively. Their decrement factors, from the results of the calculations, are 0.0154, 0.025, 0.031, and 0.0295, respectively. From the simulation results, the PV roof with the ventilation air-gap is very appropriate for the application in summer.

Table 3
Comparison of simulation results for different roofs

	A	B	C	D
Summer				
Daily solar-energy (MJ/m^2)	27.359	27.359	27.359	27.359
Daily heat-gain (MJ/m^2)	0.569	1.047	1.117	1.072
Peak cooling load (W/m^2)	8.019	15.256	16.928	16.625
Daily PV power (MJ/m^2)	1.915	1.809	1.812	–
Winter				
Daily solar-energy (MJ/m^2)	8.999	8.999	8.999	8.999
Daily heat-loss (MJ/m^2)	1.649	1.383	1.587	1.714
Peak heating load (W/m^2)	20.002	17.682	20.693	22.323
Daily PV power (MJ/m^2)	0.868	0.852	0.844	–

A – ventilated air-gap BIPV, B – non-ventilated air-gap BIPV, C – closemount BIPV, D – conventional roof.

4.1.2. The effect of the different roofs on the cooling load and PV performance

Fig. 4 represents the comparisons of hourly heat-gain and cooling-load through the different roofs. It can be seen from Fig. 4 and Table 3 that the total daily heat-gain and peak cooling-load of close contact mount BIPV (C) are slightly more than those of the normal roof D. Because of the increase of the thermal resistance, the non-ventilated air-gap BIPV slightly decreases the heat-gain and peak cooling-load in contrast with the conventional roof D. The cooling load for roof A is reduced significantly because of the PV shading and natural convection of air in the gap. Decreases of 46% and 51% occured in Table 3 for the daily heat-gain and peak cooling-load through the ventilated PV roof compared with the conventional roof D. During the evening, with no solar radiation, the loss of radiant energy to the sky can cool a roof below the ambient air temperature. So, in Fig. 4, the differences of heat gains between the three PV roofs and the roof D in the morning are relatively higher in comparison than those in the afternoon because of the PV shielding from the radiative heat-transfer between the exterior of roof and the sky.

Fig. 5 shows the hourly variations of PV temperature and PV conversion efficiency for the three types of BIPV. It is found that for the case of the PV roof with the ventilation air

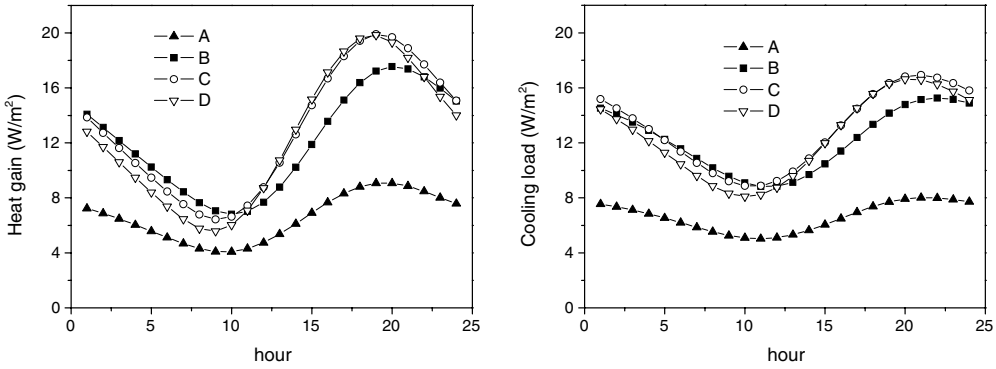

Fig. 4. Comparisons of heat gain and cooling load through the four different roofs (A – ventilated air-gap BIPV, B – non-ventilated air-gap BIPV, C – closemount BIPV, D – conventional roof).

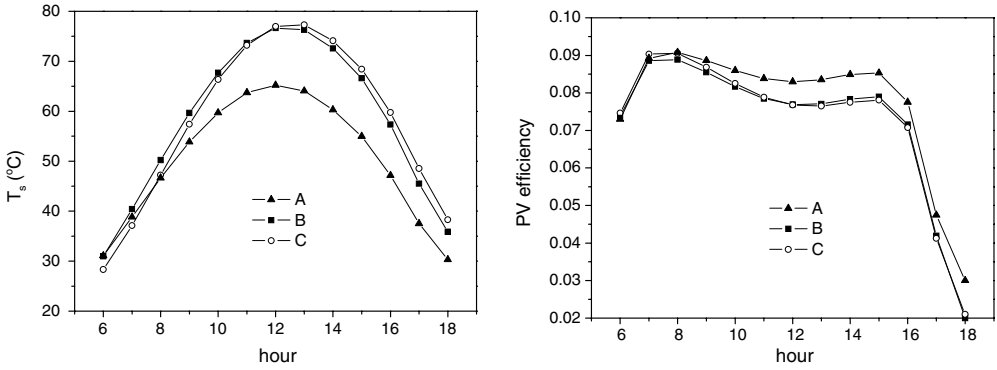

Fig. 5. Comparisons of solar cells' temperature and PV conversions for the three types of BIPV in summer (A – ventilated air-gap BIPV, B – non-ventilated air-gap BIPV, C – closemount BIPV).

gap, the PV conversion efficiency is higher than the other two cases and the reduction of maximum PV temperature in contrast to the other two types of BIPV is approximately 14 °C. Table 3 indicates that the daily total PV electrical output in the case of roof A can be increased up to 6% in comparison with the close roof mounted and closed duct BIPV. The differences of PV temperature and conversion efficiency between roof B and C are not significant. Then it is obvious that the PV with ventilation air gap is suitable for the application in summer.

4.1.3. Comparisons of heat gain between the PV ventilated roof and cool roof

The investigations conclude that the use of reflective roofs represents an attractive option to reduce space cooling-energy [24]. Fig. 6 shows the comparison of heat gain between the PV roof with the ventilation air-gap and normal roof D of different absorptivities. It is evident that the decrease of roof absorptance can lead to the reduction of heat gain through the roof. As can be seen from Fig. 6, the peak heat-gain of the PV ventilated roof has the same value as the reflective roof with an absorptivity of about 0.4. The PV ventilation roof and cool roof with absorptivity of 0.45 have the same effect on the total heat-gain over the day. It should be noted that a higher roof solar-reflectance reduces the solar energy absorbed by the roof and therefore usually provides a reduction in the cost of air conditioning, while causing the heating cost to increase [25].

4.2. Effect of the different roofs on the heating load

It is seen from Fig. 7 that the peak heating-load appears at approximately 11 AM because of the thermal time-lag of the roof heat-transfer and the reduction of peak heating load of the two PV roofs with air gaps is very significant because of the combination of the increase of thermal resistance and the effect of the shielding by the PV from the sky radiation. However, during the daytime, due to the shielding by the PV from the solar radiation that is more than the sky radiation, the differences of heat loss and heating load between roof D and roof A (or B) are relatively small by contrast with the results for the evening. In the afternoon, the heat loss and heating load for the case of the ventilated air-gap BIPV are even more than those of roof D. The thermal-time

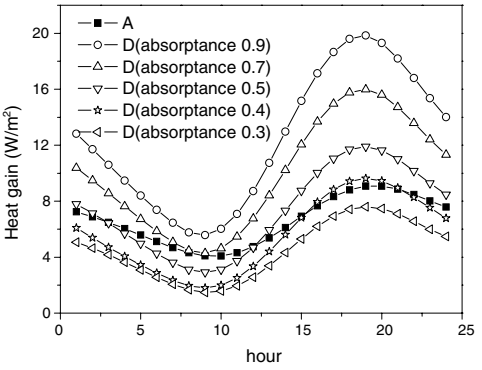

Fig. 6. Comparisons of heat gains between PV roof with ventilated air-gap and normal roof of different absorptivities (A – ventilated air-gap BIPV, D – conventional roof).

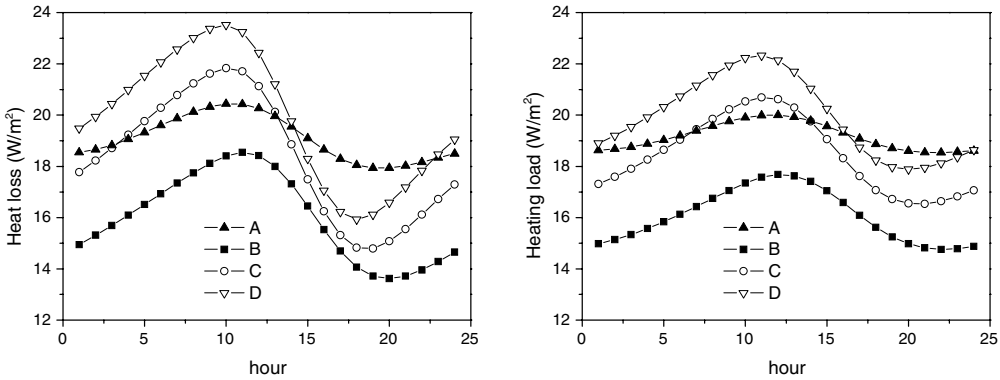

Fig. 7. Comparisons of heat losses and heating loads through the four different roofs (A – ventilated air-gap BIPV, B – non-ventilated air-gap BIPV, C – closemount BIPV, D – conventional roof).

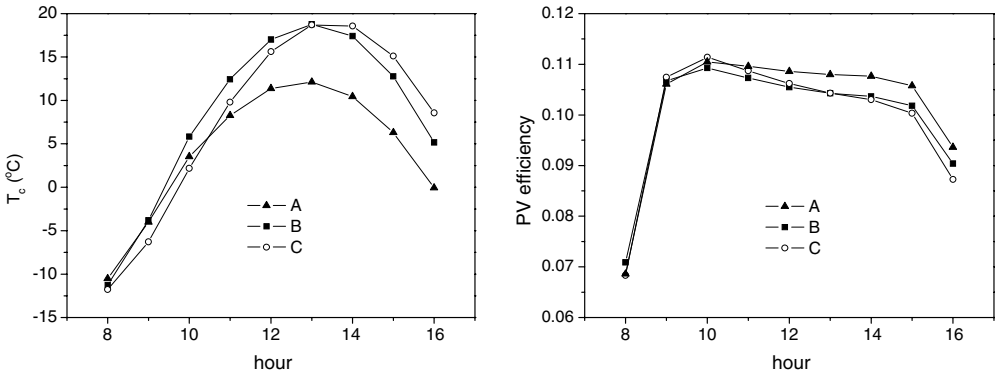

Fig. 8. Comparisons of solar cells' temperatures and PV conversions for the three types of BIPV in winter (A – ventilated air-gap BIPV, B – non-ventilated air-gap BIPV, C – closemount BIPV).

lag of the heat transfer through the roof should be taken into consideration during the above analysis.

It is found from Table 3 that the minimum daily heat-loss through the roof can be reduced by 20% in the case of the BIPV of closed air-duct compared with the conventional roof D and the maximum daily PV power output is the BIPV with the ventilated air gap. The maximum PV temperature-differences between the ventilated air-gap and the other two cases with BIPV are about 8 °C in Fig. 8 and the difference of daily PV outputs between three types of BIPV is not significant in Table 3. Then the closed air-duct BIPV is suitable for the application in winter.

5. Conclusions

The performance comparisons for the three different BIPV roofs and the conventional roof are made based on the one-dimensional transient model for Tianjin, China. In summer, the optimum method of the BIPV is the PV with the ventilated air-gap because this

integration leads to a high PV conversion efficiency and low cooling load. The PV roof with a ventilation air-gap has a high time-lag and small decrement factor in comparison with the other three roofs and has the same heat gain as the cool roof of absorptance 0.4. In winter, the appropriate integration building of PV is the non-ventilated (closed) air duct BIPV because of the combination of the low heating-load and the high PV power-output. It should be noted that the PV performance and the change of heating and cooling loads through the different roofs depend also on many other factors, such as initial roof insulation level, roof solar absorptivity, local climate, etc.

Acknowledgments

The authors thank Dr. Jeffrey Spitler from School of Mechanical and Aerospace Engineering, Oklahoma State University, for useful discussions of the RTS cooling-load model. They also gratefully acknowledge Dr. Yang Hongxing (Department of Building Services Engineering, Hong Kong Polytechnic University) for useful advice on the development of the ventilation PV roof model.

References

[1] Tu Fengxiang. Current situation and development tendency of building energy-conservation. Build Sci 2004;9:8–11 [in Chinese].
[2] Hestnes AG. Building integration of solar energy systems. Sol Energy 1999;67(4–6):181–7.
[3] Ciampi M, Leccese F, Tuoni G. Ventilated facades energy performance in the summer cooling of buildings. Sol Energy 2003;75:491–502.
[4] Brinkworth BJ, Cross BM, Marshall RH, Yang Hongxing. Thermal regulation of photovoltaic cladding. Sol Energy 1997;61:169–78.
[5] Yang HX, Burnett J, Zhu Z, Lu L. A simulation study on the energy performance of photovoltaic roofs. ASHRAE Trans 2001;107(2):129–35.
[6] Mei Li, Infield D, Eicker U, Fux V. Thermal modelling of a building with an integrated ventilated PV facade. Energy Build 2003;35:605–17.
[7] McClellan TM, Pedersen CO. Investigation of outside heat-balance models for use in a heat-balance cooling load calculation procedure. ASHRAE Trans 1997;103(2):469–84.
[8] Duffie JA, Beckman WA. Solar engineering of thermal processes. New York: Wiley; 1980.
[9] Brinkworth BJ, Marshall RH. A validated model of naturally-ventilated PV cladding. Sol Energy 2000;69(1):67–81.
[10] Afonso C, Oliveira A. Solar chimneys: simulations and experiment. Energy Build 2000;32(1):71–9.
[11] ASHRAE. ASHRAE handbook – fundamentals. Atlanta: American Society of Heating, Refrigerating and Air-Conditioning Engineers, Inc; 2001.
[12] King DL, Boyson WE, Kratochvil JA. Photovoltaic-array performance model. Albuquerque: Sandia National Laboratories; 2004.
[13] Spitler JD, Fisher DE, Pedersen CO. The radiant time-series cooling load calculation procedure. ASHRAE Trans 1997;103(2):503–15.
[14] Spitler JD. PRF-RTF Generator <www.hvac.okstate.edu> [accessed 9.05.05].
[15] Hollands KGT, Unny TE, Raithby GD, Konicek L. Free convective heat-transfer across inclined air layers. J Heat Transfer 1976;98:189–93.
[16] Yogesh J, Keneth ET. Computational heat transfer. 2nd ed. New York: Taylor & Francis; 2003.
[17] Using Simulink, 4th ed. Natick (MA): The MathWorks Inc; 2003.
[18] Davis MW, Dougherty BP, Fanney AH. Prediction of building integrated photovoltaic-cell temperatures. J Sol Energy Eng Trans ASME 2001;123(2):200–10.
[19] Garg HP, Adhikari RS. Transient simulation of convectional hybrid photovoltaic/thermal (PV/T) air-heating collectors. Int J Energ Res 1998;22:547–62.
[20] Ma ZL, Yang Y. Design of air conditioning for civil buildings. Beijing: China Chemical Industry Press; 2003 [in Chinese].

[21] Zhang QY, Huang J. Standard meteorological database for buildings in China. Beijing: China Machine Press; 2004 [in Chinese].
[22] Duffin RJ. A passive-wall design to minimize building temperature swings. Sol Energy 1984;33:337–42.
[23] Asan H. Effects of wall's insulation thickness and position on time lag and decrement factor. Energy Build 1998;28:299–305.
[24] Parker DS, Barkaszi SF. Roof solar reflectance and cooling energy use: field research results from Florida. Energy Build 1997;25:105–15.
[25] Griggs EI, Sharp TR, MacDonald JM. Guide for estimating differences in a building's heating and cooling energy due to changes in solar reflectance of a low-sloped roof. ORNL-6527; 1989.